




# Solution Phase Limited Diffusion Modeling in a Li-ion Cell Subject to Concentration-Dependent Pore Wall Flux

Girish Krishnan,<sup>1</sup> Mohammad Parhizi,<sup>1</sup> Manan Pathak,<sup>2</sup> and Ankur Jain<sup>1,z</sup> 

<sup>1</sup>Mechanical and Aerospace Engineering Department University of Texas at Arlington, Arlington, Texas United States of America

<sup>2</sup>BattGenie Inc., Seattle, Washington, United States of America

Mathematical modeling of ionic transport in a Li-ion cell is critical for understanding and predicting key performance parameters such as cell voltage. Past work on solution phase limitation modeling of a Li-ion cell has assumed constant and uniform pore wall flux, which is valid only under certain conditions. It may be more appropriate to assume, similar to chemical reactions in general, that the pore wall flux is proportional to the local ion concentration. This paper presents a theoretical model for solution phase limited ionic diffusion in a separator-electrode stack under the assumption of the pore wall flux being linearly proportional to the local concentration. The resulting non-linear governing equation is linearized and solved using Laplace transformation technique. Concentration field in the two-layer stack is calculated as a function of space and time in a parameter space of practical interest. A comparison of results with past work based on constant, uniform reaction rate indicates that the assumed nature of concentration-dependence of the pore wall flux plays a significant role in determining the concentration distribution. This work advances the theoretical understanding of ionic diffusion in a Li-ion cell, and may contribute towards understanding and optimizing the performance of Li-ion cells.

© 2021 The Electrochemical Society ("ECS"). Published on behalf of ECS by IOP Publishing Limited. [DOI: [10.1149/1945-7111/ac1cfb](https://doi.org/10.1149/1945-7111/ac1cfb)]

Manuscript submitted April 9, 2021; revised manuscript received July 25, 2021. Published September 6, 2021.

## List of symbols

$a$	Specific interfacial area ( $\text{m}^{-1}$ )
$C$	Concentration ( $\text{mol m}^{-3}$ )
$C_o$	Reference concentration ( $\text{mol m}^{-3}$ )
$c$	Non-dimensional concentration, $c = C/C_o$
$\hat{c}$	Laplace transform of non-dimensional concentration
$D$	Diffusion coefficient of electrolyte ( $\text{m}^2 \text{s}^{-1}$ )
$C_{in}(x)$	Initial concentration distribution ( $\text{mol m}^{-3}$ )
$f(x)$	Non-dimensional initial concentration distribution, $f(x) = F(x)/C_o$
$F$	Faraday's constant ( $\text{C mol}^{-1}$ )
$I$	Current density ( $\text{A m}^{-2}$ )
$j_n$	Pore wall flux ( $\text{mol m}^{-2} \text{s}^{-1}$ )
$J$	Non-dimensional pore wall flux, $J = -I(1 - t_+)/L_s^2/FL_cDC_o$
$L_s$	Length of separator (m)
$L_c$	Length of porous electrode (m)
$r$	Electrode length to separator length ratio, $r = L_c/L_s$
$s$	Laplace variable
$t_+$	Transference number
$t$	Non-dimensional time, $t = Dt/L_s^2$
$X$	Length scale (m)
$x$	Non-dimensional length scale, $x = X/L_s$
$\varepsilon$	Porosity
$\tau$	Time (s)
Subscripts	
1	Separator
2	Electrode

Li-ion cells are used extensively for electrochemical energy storage and conversion in a variety of engineering applications, such as renewable energy storage and electric-based transportation.<sup>1,2</sup> In these and several other applications, maintaining high energy conversion efficiency and reliability over a large number of cycles is critical.<sup>3,4</sup> Mathematical modeling of Li-ion diffusion within the cell is critical for understanding the nature of electrochemical energy conversion and to ultimately optimize these processes towards high efficiency and reliability.<sup>5,6</sup>

A very comprehensive body of literature already exists on the mathematical modeling of diffusion and electrochemical processes

in a Li-ion cell subject to different operating conditions.<sup>7,8</sup> Mathematical modeling of Li-ion batteries involves conservation of mass, charge, and energy equations coupled with kinetic reactions.<sup>7,9</sup> A robust and widely used electrochemical model is the Pseudo-2D model (P2D) that has been developed based on the porous electrode theory<sup>10</sup> and the concentrated solution theory.<sup>11</sup> Exact solutions do not exist for P2D models due to the non-linear and coupled nature of the transport equations and Butler-Volmer kinetics. Thus, P2D models are commonly solved using numerical approaches that often result in a large number of equations due to spatial discretization, and consequently take significant computational effort to solve.<sup>12</sup> Much research has been reported on developing fast numerical methods to solve P2D models.<sup>12,13</sup> In order to understand the behavior of the battery under various limiting conditions, early work by Doyle & Newman<sup>14</sup> proposed three major limiting cases including solid-phase diffusion limitation, solution-phase diffusion limitation, and an ohmically-limited cell in which open-circuit potential depends linearly on state of charge. In the solid-phase limitation, lithium ions in the electrolyte are assumed to diffuse rapidly through the electrolyte, and diffusion through the electrode material particle, modeled by a representative sphere is the rate-limiting step. The solid-phase limitation is the basis of a simplified model called Single Particle Model (SPM) that has been used extensively in the past.<sup>7</sup> SPM neglects concentration and potential gradients in the electrolyte phase and assumes a uniform distribution of the current density throughout the length of the electrodes.<sup>15,16</sup> These assumptions are valid at relatively low charge/discharge rates and thin electrodes.<sup>17</sup> A variety of analytical, approximate and numerical techniques have been used to solve SPM problems under different operating conditions. Some of these include the separation of variables approach for single layer<sup>14</sup> and multi-layer electrodes under galvanostatic boundary conditions,<sup>18</sup> Laplace transformation technique,<sup>19,20</sup> Green's function for single and multi-layer electrodes under time-dependent current density<sup>21</sup> and extended SPM accounting for effect of electrolyte concentration and potential.<sup>22,23</sup> On the other hand, modeling of the solution phase limitation regime involves modeling the transport of lithium ions through the electrolyte phase due to gradients in concentration and potential, by solving the equations governing conservation of mass and charge in the solution phase of a cell.<sup>14,24,25</sup>

In the solution phase limitation modeling of a separator-electrode geometry, influx/outflow of Li ions at the separator end of the two-layer geometry is counteracted by consumption/generation in the electrode layer due to intercalation/deintercalation. Early work on

<sup>z</sup>E-mail: [jaina@uta.edu](mailto:jaina@uta.edu)

solution phase limitation modeling in a Li-ion cell<sup>14</sup> has been followed by further work specifically on two-layer<sup>24</sup> and three-layer geometries<sup>25</sup> using separation of variables technique. Laplace transform technique has also been used to determine the concentration profile for the solution-phase diffusion limitation.<sup>20</sup> Green's function approach has been used to solve the material balance in the electrolyte for a constant uniform reaction rate.<sup>26</sup> Later, analytical solution has been presented for the case of a two-layer porous electrode with a spatially uniform but time-dependent reaction rate using Green's function approach.<sup>27</sup> Most of the literature on solution phase limitation modeling assumes constant and uniform pore wall flux in the electrode. According to Doyle & Newman,<sup>14</sup> this assumption is valid when kinetic resistances dominate ohmic resistances. Such an assumption results in a uniform and constant consumption/generation term in the governing conservation equations, which can be easily handled by analytical methods such as separation of variables. At the other end of the spectrum, Doyle & Newman<sup>14</sup> also discussed the Stein analysis, in which, the reaction is assumed to occur only very close to the electrode-separator interface. Analytical results were derived for this extreme scenario and compared with the uniform pore wall flux model.<sup>14</sup>

Uniform pore wall flux and Stein analysis are two extreme scenarios, which may be valid only under certain assumptions. For example, uniform pore wall flux is expected to be reasonably valid when the open circuit potential of the insertion material depends strongly on the state of charge of the system<sup>28</sup> or when kinetic resistances dominate ohmic resistances.<sup>14</sup> On the other hand, Stein analysis is representative of an ohmically-limited system or very large rates. Between these two extremes, it may be desirable to model the pore wall flux as being proportional to the local concentration instead of being either uniform throughout or limited only to a small thickness near the electrode-separator interface. In general, the rate of any chemical reaction depends on the reactant concentration, with a linear, first-order relationship being common for many systems.<sup>29</sup> Accordingly, it is of interest to model pore wall flux as being proportional to the local concentration in solution phase limitation modeling of a Li-ion cell. Specifically, a linear dependence of pore wall flux on the local concentration may be representative of first-order reaction kinetics.

This paper presents solution phase limitation modeling of a two-layer cell under the general assumption of pore wall flux being proportional to the local concentration. It is shown that modeling of the pore wall flux as being linearly concentration-dependent results in a non-linear integro-differential equation for the concentration field. A semi-analytical method based on linearization over small time steps followed by the use of Laplace transformation is shown to result in an accurate prediction of the concentration field. Results are found to be in good agreement with finite-difference simulation results. A comparison of the results with past results based on the uniform pore wall flux model is presented. The impact of this assumption on the concentration distribution is examined. The effect of various problem parameters on the concentration field is also discussed.

## Mathematical Modeling

**Problem statement and non-dimensionalization.**—Figure 1 shows a Li-ion cell stack considered in this paper, comprising a separator and a porous electrode, with a Li foil electrode on the left of the separator. The porous electrode is considered to be a cathode, so that a positive current density implies cell discharge, in which, species consumption occurs in the porous electrode. Governing conservation equations for the two-layer structure can be written based on a balance between diffusion, consumption/generation and transient terms. Note that the migration term can be neglected based on the commonly made assumption of constant transference number  $t_+$ . Also, tortuosity effects in the separator are neglected. The tortuosity effects in the cathode are modeled through the commonly used Bruggemann correlation and a value of 3/2 for the Bruggemann coefficient is used in this work.

These assumptions result in the following equations for concentration fields in the two layers,  $C_1$  and  $C_2$ :

$$D \frac{\partial^2 C_1}{\partial X^2} = \frac{\partial C_1}{\partial \tau} \quad 0 < X < L_s \quad [1]$$

$$D \varepsilon^{3/2} \frac{\partial^2 C_2}{\partial X^2} + a j_n (1 - t_+) = \varepsilon \frac{\partial C_2}{\partial \tau} \quad L_s < X < L_s + L_c \quad [2]$$

where  $j_n$ ,  $a$  and  $t_+$  are the pore wall flux, specific interfacial area and transference number, respectively.  $D$  and  $\varepsilon$  are the electrolyte diffusivity and electrode porosity, respectively.

Associated boundary conditions are as follows:

$$\left( \frac{\partial C_1}{\partial X} \right)_{X=0} = -\frac{I(1-t_+)}{FD} \quad \text{at } X=0 \quad [3]$$

$$C_1 = C_2 \quad \text{at } X = L_s \quad [4]$$

$$\left( \frac{\partial C_1}{\partial X} \right)_{X=L_s} = \varepsilon^{3/2} \left( \frac{\partial C_2}{\partial X} \right)_{X=L_s} \quad \text{at } X = L_s \quad [5]$$

$$\left( \frac{\partial C_2}{\partial X} \right)_{X=L_s+L_c} = 0 \quad \text{at } X = L_s + L_c \quad [6]$$

where  $F$  is the Faraday number and  $I$  is the applied current density.  $L_s$  and  $L_c$  are the lengths of the separator and electrode, respectively.

An arbitrary initial concentration distribution is assumed as follows:

$$C_1 = C_{in,1}(X) \quad \text{at } \tau = 0 \quad [7]$$

$$C_2 = C_{in,2}(X) \quad \text{at } \tau = 0 \quad [8]$$

Based on species conservation, the pore wall flux and current density are related to each other as follows:

$$-aF \int_{L_s}^{L_s+L_c} j_n(X) dX = I \quad [9]$$

Unlike past work,<sup>14,24,25</sup> in which, a uniform pore wall flux was assumed, the present work assumes that the pore wall flux is proportional to a power of the local concentration. Specifically, it is assumed that

$$j_n = \frac{1}{A} (C_2)^n \quad [10]$$

where  $n$  is the order of proportionality. For  $n = 1$ , the pore wall flux is linearly dependent on concentration, corresponding to first-order kinetics. Inserting Eq. 10 in Eq. 9 results in the following expression for  $A$ , the constant of proportionality:

$$A = \frac{aF}{I} \int_{L_s}^{L_s+L_c} [C_2(X, \tau)]^n dX = \frac{aFL_c}{I} \bar{C}_{2,n}(\tau) \quad [11]$$

where  $\bar{C}_{2,n} = \frac{1}{L_c} \int_{L_s}^{L_s+L_c} [C_2(X, \tau)]^n dX$  in Eq. 11 may be interpreted as the  $n^{\text{th}}$  order mean concentration in the electrode. Using Eqs. 11 and 10 in the governing equation for  $C_2$  results in:

$$D \varepsilon^{3/2} \frac{\partial^2 C_2}{\partial X^2} + \frac{I(1-t_+)}{FL_c} \frac{(C_2)^n}{\bar{C}_{2,n}} = \varepsilon \frac{\partial C_2}{\partial \tau} \quad L_s < X < L_s + L_c \quad [12]$$

Note that  $n = 1$  corresponds to first-order reaction kinetics, in which case,  $\bar{C}_{2,1}$  is simply the average concentration in the electrode. This is the case considered in the rest of the paper, and for convenience,  $\bar{C}_{2,1}$  is

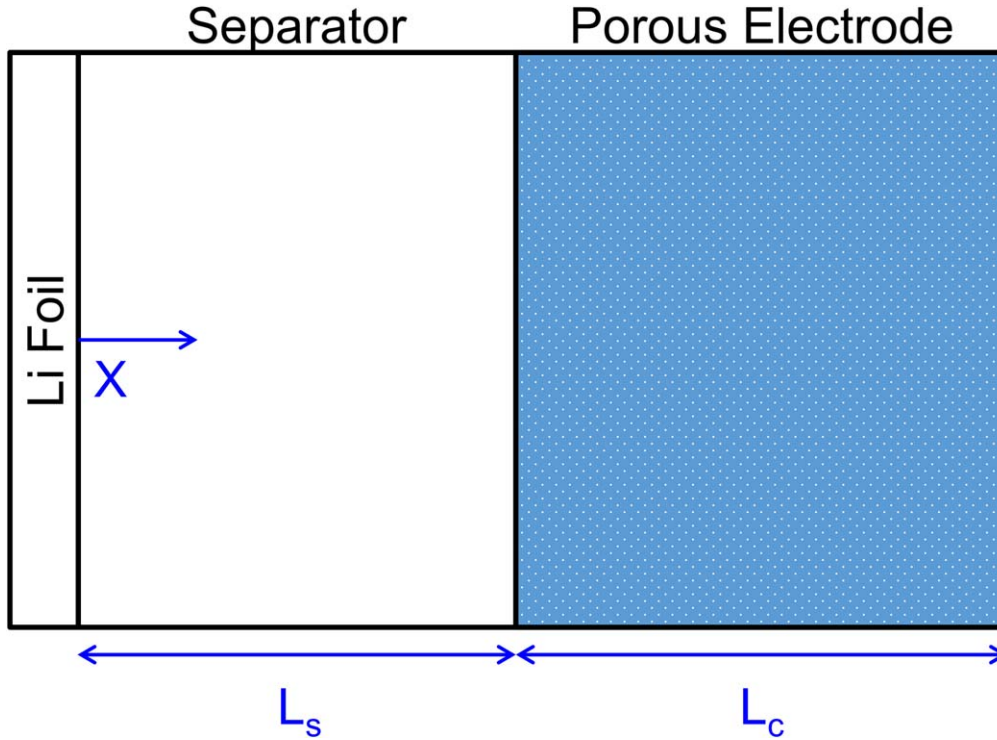


**Figure 1.** Schematic of the composite porous electrode consisting of Li foil, separator, and positive porous electrode.

simply written as  $\bar{C}_2$ . Further, note that the treatment above reduces to the commonly-used uniform pore wall flux case for  $n = 0$ .

In order to ensure generality of results, it is useful to carry out non-dimensionalization using the following set of parameters:

$$c = C/C_0; J = -\frac{I(1-t_+)L_s^2}{FL_cDC_0}; t = \frac{D\tau}{L_s^2}; r = \frac{L_c}{L_s}; x = \frac{X}{L_s};$$

$$f_1(x) = \frac{C_{in,1}(X)}{C_0}; f_2(x) = \frac{C_{in,2}(X)}{C_0} \quad [13]$$

The resulting set of non-dimensional governing equations are

$$\frac{\partial^2 c_1}{\partial x^2} = \frac{\partial c_1}{\partial t} \quad 0 < x < 1 \quad [14]$$

$$\varepsilon^{1/2} \frac{\partial^2 c_2}{\partial x^2} + \beta J c_2 = \frac{\partial c_2}{\partial t} \quad 1 < x < 1 + r \quad [15]$$

where  $\beta = (\varepsilon \bar{c}_2)^{-1}$  and  $\bar{c}_2 = \frac{1}{r} \int_1^{1+r} c_2 dx$ .

The non-dimensionalized boundary conditions are:

$$\left( \frac{\partial c_1}{\partial x} \right) = Jr \quad \text{at } x = 0 \quad [16]$$

$$c_1 = c_2 \quad \text{at } x = 1 \quad [17]$$

$$\left( \frac{\partial c_1}{\partial x} \right) = \varepsilon^{3/2} \left( \frac{\partial c_2}{\partial x} \right) \quad \text{at } x = 1 \quad [18]$$

$$\left( \frac{\partial c_2}{\partial x} \right) = 0 \quad \text{at } x = 1 + r \quad [19]$$

and the initial conditions are:

$$c_1 = f_1(x); c_2 = f_2(x) \quad \text{at } t = 0 \quad [20]$$

Equation 15 is a non-linear partial differential equation, since the parameter  $\beta$  itself depends on the concentration field, and therefore is a function of time. Further, a spatial integral of the concentration field appears in the  $\beta$  term. As a result, this set of equations cannot be solved using standard analytical tools such as the separation of variables method.

**Solution procedure.**—A timestepping-based semi-analytical technique is used to solve the non-linear set of equations derived in the previous sub-section. The time domain of interest is split into a number of equal time steps,  $\Delta t$ . In each time step,  $\beta$  is approximated to be constant, so that Eqs. 14–20 are linearized and solved within that time step. The value of  $\beta$  for the first time step is determined using the initial condition. For example, for a uniform initial concentration,  $c_2 = 1$ ,  $\beta$  is simply given by  $\beta = 1/\varepsilon$ . The value of  $\beta$  for any subsequent timestep is calculated by determining and integrating the concentration field at the end of the previous time interval. In this manner, the solution marches forward in time in a recursive manner with a time step of  $\Delta t$  until the desired total time is reached.

In order to carry out this recursive technique for solving the problem, an analytical solution for the transient concentration field over a time  $\Delta t$  with constant  $\beta$  is needed. A solution for this problem using the Laplace transformation technique is discussed in the next sub-section.

**Laplace transform solution for the sub-problem.**—Assuming constant  $\beta$  within a certain timestep, carrying out Laplace transform on Eqs. 14–19 results in the following set of equations in the Laplace domain:

$$\frac{d^2 \widehat{c}_1}{dx^2} = s \widehat{c}_1 - c_{1,in}(x) \quad [21]$$

$$\varepsilon^{1/2} \frac{d^2 \widehat{c}_2}{dx^2} + \beta J \widehat{c}_2 = s \widehat{c}_2 - c_{2,in}(x) \quad [22]$$

where  $\widehat{c}_1$  and  $\widehat{c}_2$  are Laplace transforms of  $c_1$  and  $c_2$ ,  $s$  is the Laplace variable, and  $c_{1,in}(x)$  and  $c_{2,in}(x)$  are the initial concentration distributions at the start of the timestep, which are obtainable from the solution of the previous timestep.

The relevant boundary and interface conditions in the Laplace domain are as follows:

$$\frac{d\widehat{c}_1}{dx} = \frac{rJ}{s} \quad \text{at } x = 0 \quad [23]$$

$$\widehat{c}_1 = \widehat{c}_2 \quad \text{at } x = 1 \quad [24]$$

$$\frac{d\widehat{c}_1}{dx} = \varepsilon^{3/2} \frac{d\widehat{c}_2}{dx} \quad \text{at } x = 1 \quad [25]$$

$$\frac{d\widehat{c}_2}{dx} = 0 \quad \text{at } x = 1 + r \quad [26]$$

In order to solve the ordinary differential equations given by Eqs. 21 and 22, the initial concentration distributions  $c_{1,in}(x)$  and  $c_{2,in}(x)$  are fitted with a quadratic fit, i.e.

$$c_{1,in}(x) = a_1x^2 + b_1x + c_1 \quad [27]$$

$$c_{2,in}(x) = a_2x^2 + b_2x + c_2 \quad [28]$$

Subsequently, the solutions for  $\widehat{c}_1$  and  $\widehat{c}_2$  from Eqs. 21 and 22 are given by

$$\widehat{c}_1 = \frac{2a_1}{s^2} + \frac{a_1x^2 + b_1x + c_1}{s} + A_1 \exp(\gamma_1x) + B_1 \exp(-\gamma_1x) \quad [29]$$

$$\widehat{c}_2 = \frac{2\sqrt{\varepsilon}a_2}{(s - \beta J)^2} + \frac{a_2x^2 + b_2x + c_2}{s - \beta J} + A_2 \exp(\gamma_2x) + B_2 \exp(-\gamma_2x) \quad [30]$$

where  $\gamma_1 = \sqrt{s}$  and  $\gamma_2 = \sqrt{\frac{s - \beta J}{\varepsilon}}$ .

Boundary and interface conditions given by Eqs. 23–26 can be used to determine the four unknown coefficients in Eqs. 29–30 as follows:

$$X = P^{-1}Q \quad [31]$$

where

$$P = \begin{bmatrix} 1 & -1 & 0 & 0 \\ \exp(\gamma_1) & \exp(-\gamma_1) & -\exp(\gamma_2) & -\exp(-\gamma_2) \\ \gamma_1 \exp(\gamma_1) & -\gamma_1 \exp(-\gamma_1) & -\varepsilon^{3/2}\gamma_2 \exp(\gamma_2) & \varepsilon^{3/2}\gamma_2 \exp(-\gamma_2) \\ 0 & 0 & \exp(\gamma_2(1+r)) & -\exp(-\gamma_2(1+r)) \end{bmatrix} \quad [32]$$

$$Q = \begin{bmatrix} \frac{rJ - b_1}{s^{3/2}} \\ \frac{s(a_2 + b_2 + c_2) - (s - \beta J)(a_1 + b_1 + c_1)}{s(s - \beta J)} + \frac{2\sqrt{\varepsilon}a_2s^2 - 2a_1(s - \beta J)^2}{s^2(s - \beta J)^2} \\ \frac{\varepsilon^{3/2}(2a_2 + b_2) - (2a_1 + b_1)(s - \beta J)}{s(s - \beta J)} \\ \frac{-(2a_2(1+r) + b_2)}{\gamma_2(s - \beta J)} \end{bmatrix} \quad [33]$$

$$X = \begin{bmatrix} A_1 \\ B_1 \\ A_2 \\ B_2 \end{bmatrix} \quad [34]$$

For the initial time step, based on a uniform initial concentration,  $a_1$ ,  $b_1$ ,  $a_2$  and  $b_2$  are set to be equal to zero, whereas  $c_1$  and  $c_2$  are set to be equal to one.

The solution of the concentration field in the Laplace domain, given by Eqs. 29 and 30 needs to be inverted in order to determine concentrations in the separator and electrode as functions of space and time. Due to the complicated nature of these expressions, particularly the coefficients, it is unlikely that an analytical inversion is possible. Instead, a numerical inversion technique<sup>30</sup> based on de Hoog's quotient difference method<sup>31</sup> is used to determine  $c_1(x,t)$  and  $c_2(x,t)$ .

## Results and Discussion

**Verification of the solution methodology.**—The solution methodology is verified through comparison with a finite-difference based numerical simulation. The numerical simulation is carried out by discretizing the governing equations and solving for concentration at each node corresponding to a time step using an implicit scheme. The central difference formula is used to approximate the spatial derivatives in the governing equations which results in a set of coupled algebraic equations. The resulting algebraic equations are solved using a Tri-Diagonal Matrix Algorithm (TDMA). A total number of 1000 spatial nodes and 1000 time intervals are found to ensure that the solution is independent of mesh size and timestep. This comparison is presented in Fig. 2, where concentrations at multiple points are plotted as function of time in Fig. 2a and concentration distributions are plotted at multiple times in Fig. 2b. The problem parameters are  $r = 5$ ,  $J = -0.0096$  and  $\varepsilon = 0.35$ . The value of the non-dimensional pore wall flux,  $J$ , is computed using Eq. 13 and corresponding parameter values from Table I for a current density of  $80 \text{ A m}^{-2}$ . The values listed in Table I are taken from past work<sup>21</sup> except the transference number, for which, a value of 0.4 is assumed in all Figures, unless specified otherwise. Results from both Laplace transform based technique and numerical simulations are plotted. In general, there is very good agreement between the two at multiple points and at different times. The worst-case deviation between the two is 0.4%, which can be considered as extremely low for most engineering applications. Note that there may be residual error due to discretization in the numerical simulation. Further, in the Laplace transform approach, numerical inversion of the solutions in Laplace domain using de Hoog's method may also result in some error. A very fine discretization of 50 is specified in order to minimize such error, with no appreciable change in results observed upon further refinement. Finally, discretization into finite timesteps and assumptions of constant  $\beta$  over each timestep are also potential sources of error. Despite such sources of error, Fig. 2 shows excellent agreement between the present work and numerical simulations.

The fundamental nature of the predicted concentration field is investigated in Figs. 3 and 4. The evolution of concentration at four locations over time, starting with the uniform initial concentration is plotted in Fig. 3. The applied current is  $80 \text{ A m}^{-2}$  and values of other problem parameters are the same as in Fig. 2. Note that unlike past work, species consumption in the present work is linearly proportional to the local concentration. Figure 3 presents the evolution of concentration with time at various locations in the two-layer structure. As expected, concentration at the left boundary ( $x = 0$ ) and separator-electrode interface ( $x = 1$ ) increase with time, since species influx dominates over consumption, whereas concentration decreases with time at the center of the electrode ( $x = 1 + r/2$ ) and at the right boundary ( $x = 1 + r$ ). At each location, a steady state is

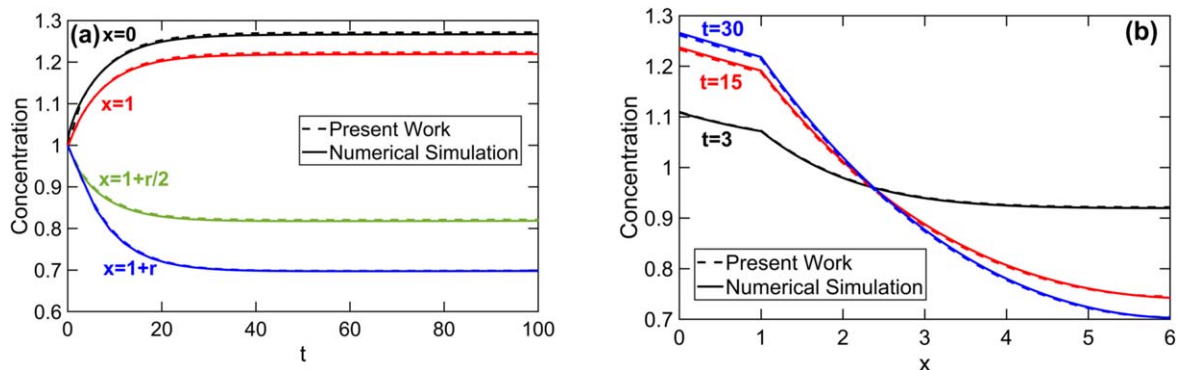


**Figure 2.** Comparison of Laplace transform based technique (present work) with finite-difference numerical simulation results: (a)  $c$  as a function of  $t$  at multiple locations; (b)  $c$  as a function of  $x$  at  $t = 3, 15$  and  $30$ .

**Table I. Electrochemical and physical properties used in this study.**

Parameter	Value	Unit
$D$	$2.6 \times 10^{-10}$	$\text{m}^2 \text{s}^{-1}$
$F$	96,487	$\text{C mol}^{-1}$
$t_+$	0.4	—
$\varepsilon$	0.35	—
$L_s$	$25 \times 10^{-6}$	m
$L_c$	$125 \times 10^{-6}$	m
$C_o$	1000	$\text{mol m}^{-3}$

reached with roughly the same time constant. For any point in the electrode, at steady state, species influx is balanced by concentration-dependent consumption and diffusion, resulting in no further change in concentration with time. On the other hand, steady state in the separator is governed by a balance between diffusion and influx from the boundary.

Curves plotted in Fig. 4 show that, as time passes, concentration increases in the separator and in the electrode region close to the separator-electrode interface due to species influx from the left boundary. Simultaneously, consumption in the remaining electrode region results in reduction in concentration. As the local concentration at a point increases (or decreases), so does the rate of species consumption, which counteracts the change in concentration, eventually leading to steady state. Interestingly, at a specific point in the electrode, consumption and influx appear to balance each other out, resulting in the concentration remaining close to the initial value throughout.

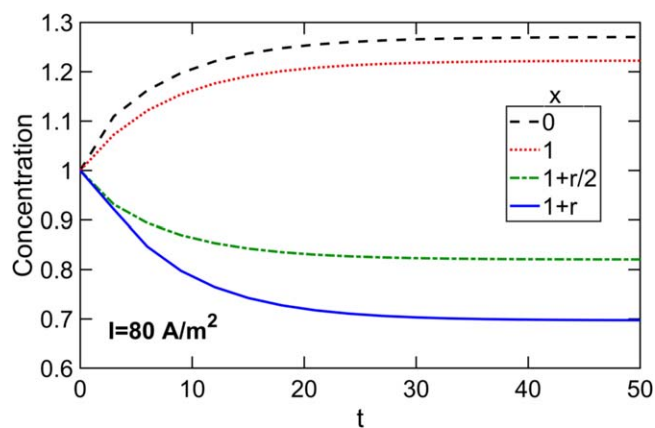


**Figure 3.** Concentration as a function of time at various locations for  $I = 80 \text{ A m}^{-2}$ .

It is instructive to compare results from the present approach, in which pore wall flux is proportional to the local concentration, with past work,<sup>21</sup> in which a uniform pore wall flux is assumed. Figure 5 presents this comparison in terms of concentration distributions at four different times, while Fig. 6 compares the two approaches in terms of concentration profiles over time at four locations. A current density of  $120 \text{ A m}^{-2}$  and a transference number of 0.2 is used in order to maintain consistency with assumptions in the past work. All other parameters remain unchanged and are identical in the two approaches.

Figures 5a–5d show that as time increases, concentration distribution predicted by the linear rate model considered in this work begins to deviate from the constant rate models used in past papers. Specifically, concentration in a region close to the electrode boundary is greater for the linear rate model, and this region grows as time increases. In the rest of the geometry, i.e., in the separator and regions of the electrode close to the interface, concentration predicted by the linear rate assumption is lower than for the constant rate assumption. This is explained on the basis of the rate of consumption in electrode being proportional to the local concentration. For example, Fig. 5a shows that the non-dimensional concentration towards the end of the electrode drops slightly from the initial value for both constant rate and linear rate cases. Therefore, at this instance, the consumption rate in the linear rate case starts deviating from the constant rate case as the consumption depends on the local concentration. At the same instance, in case of the constant rate case the consumption rate still remains the same as it was in the beginning. This trend can be clearly noticed in Fig. 5b. Since there is a continuous influx of Li ions and the consumption depends on the local concentration for the linear rate case, consumption in the electrode region closer to the separator for the linear rate case is

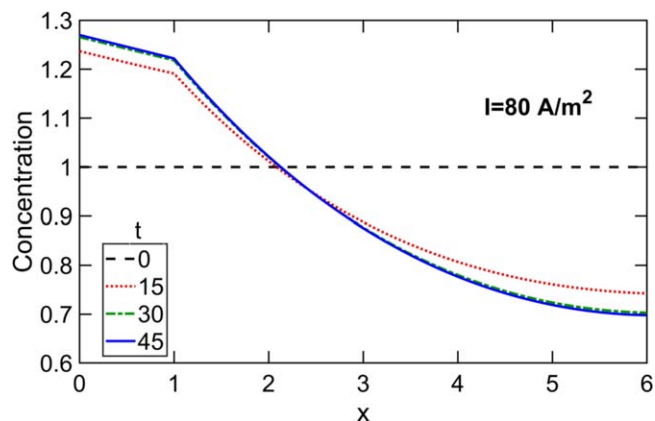


**Figure 4.** Concentration distribution in the separator-electrode structure at various times for  $I = 80 \text{ A m}^{-2}$ . Values of problem parameters are the same as for Fig. 2.

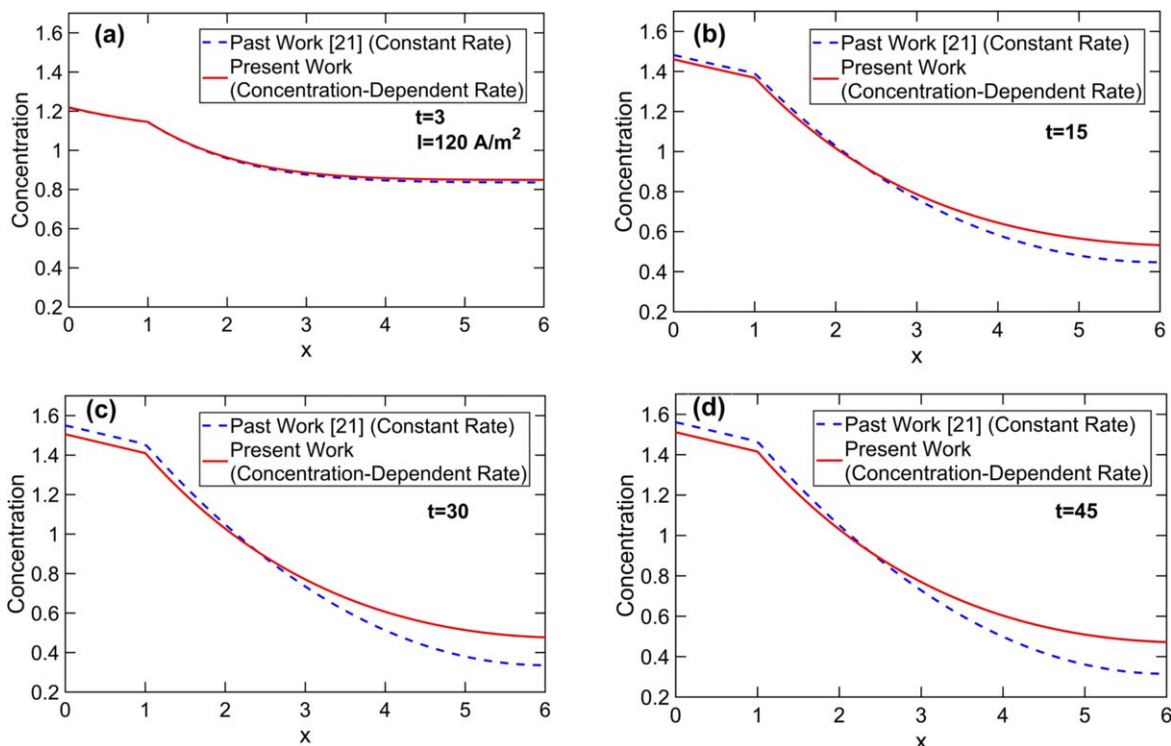


**Figure 5.** Comparison between present work based on concentration-dependent reaction rate model with past work<sup>21</sup> based on constant reaction rate assumption for  $t_+ = 0.2$  and  $I = 120 \text{ A m}^{-2}$ ;  $c$  as a function of  $x$  at (a)  $t = 3$ , (b)  $t = 15$ , (c)  $t = 30$ , (d)  $t = 45$ .

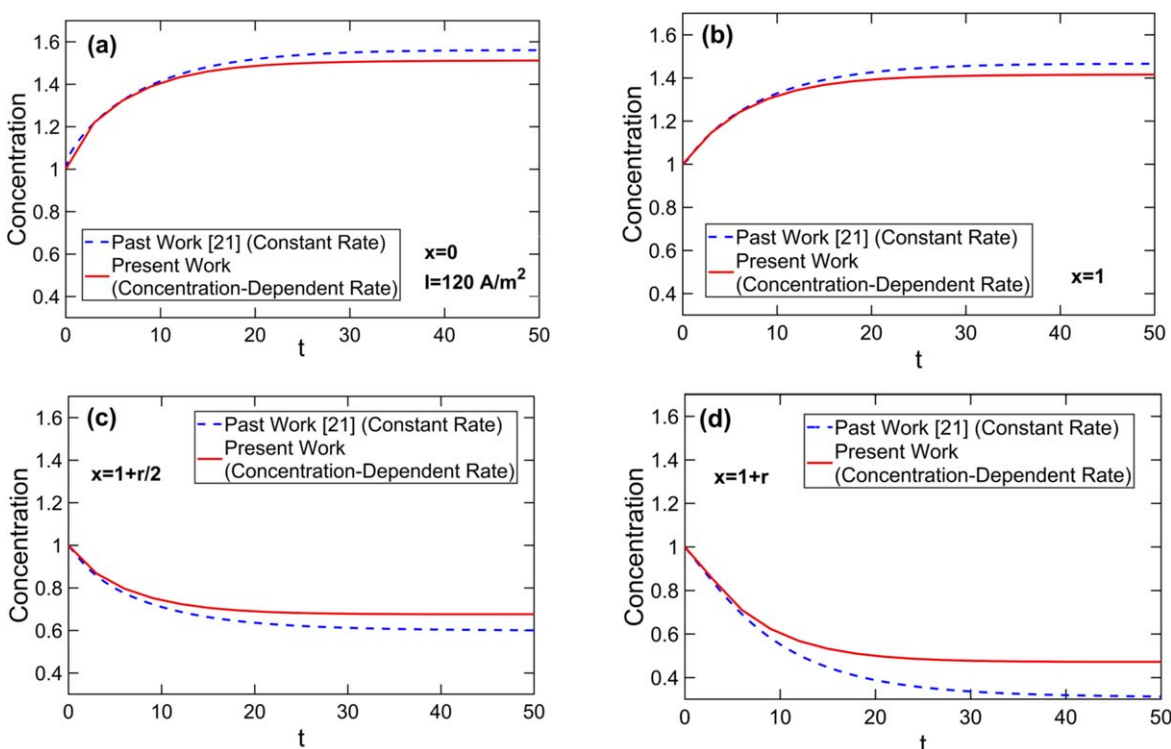
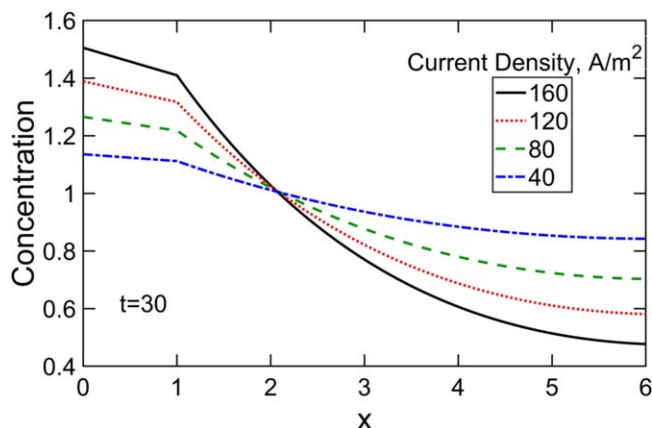


**Figure 6.** Comparison between concentration-dependent reaction rate model with past work<sup>21</sup> based on constant reaction rate assumption for  $t_+ = 0.2$  and  $I = 120 \text{ A m}^{-2}$ ;  $c$  as a function of  $t$  at (a)  $x = 0$ , (b)  $x = 1$ , (c)  $x = 1 + r/2$ , (d)  $x = 1 + r$ .

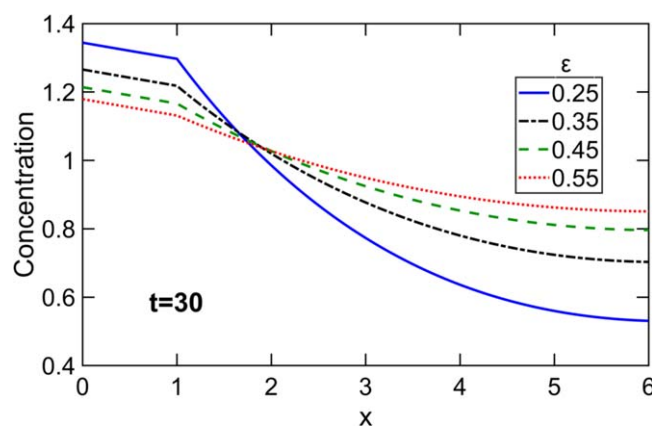
always higher at every instance, when compared with the constant rate case, which explains the reduced concentration in this region for the linear rate model compared to the constant rate model.

Figure 6 provides further comparison of results from the linear rate model with constant rate model. It is seen that for  $x = 0$  and

$x = 1$ , the predicted concentration using the linear rate model is lower than the constant rate model. This is because in the separator and in the electrode close to the interface, influx of ions due to the applied current results in an increase in concentration, which, in the linear rate model results in greater consumption in the electrode



**Figure 7.** Effect of current density on concentration distribution:  $c$  as a function of  $x$  at  $t = 30$  for multiple values of current density.



**Figure 8.** Effect of porosity on concentration distribution:  $c$  as a function of  $x$  at  $t = 30$  for multiple values of porosity.

relative to the constant rate model, which explains the results in Figs. 6a–6b. On the other hand, at the middle of the electrode and electrode boundary, the reduced concentration results in a lower rate of consumption in the linear rate model compared to the constant rate model, which is why, the linear rate curve lies above the constant rate curve in Figs. 6c–6d. It is seen that at each point, steady state is reached faster in the linear rate case. This is because the  $\beta$  term associated with the linear rate case keeps adjusting the consumption rate and at a certain instance, the adjustment results in the influx of Li ions becoming equal to the consumption rate. At this instance, the consumption rate in the constant rate case is still not equal to the influx of Li ions.

The impact of various problem parameters on the predicted concentration distribution under concentration-dependent pore wall flux is examined in the next three Figures. Figure 7 plots the concentration distribution at  $t = 30$  for four different values of current density. Other problem parameters are the same as for Fig. 2. As expected, the larger the current, the greater is the rate of influx in the separator, and therefore, the higher is the concentration distribution in the separator, as well as the electrode region close to the separator. In addition, a larger current also results in greater pore wall flux in the electrode, resulting in greater reduction in concentration at higher current density values.

The effect of porosity is discussed in Fig. 8, where concentration distribution is plotted at  $t = 30$  for four different values of the porosity. As porosity increases, the amount of Li ions entering the electrode is higher because higher porosities would result in more space available for the diffusion. Therefore, the concentration in the electrode away from the interface is greater for higher porosities. At the same time, concentration in the separator and the electrode close

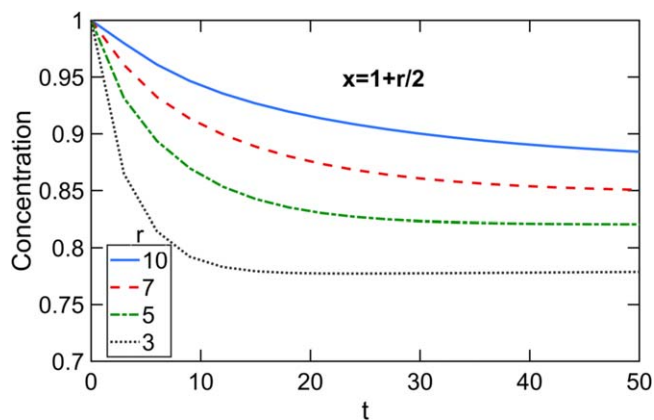


**Figure 9.** Effect of geometry on concentration distribution:  $c$  as a function of  $t$  at the center of the electrode for multiple values of  $r$ .

to the separator decreases as porosity increases. This is because higher porosity results in an increased diffusion of Li ions into the electrode as pointed out above. Therefore, for lower porosities, this would result in a greater accumulation of Li ions in the separator and electrode close to the separator. Further, Eq. 18 indicates that a greater porosity should result in lower slope of concentration distribution in the electrode at the interface relative to the slope in the separator at the interface. This is clearly seen in Fig. 9, in which, the slope at the interface in the separator is roughly the same for each porosity, but the slope in the electrode goes down as porosity increases.

The final parameter of interest in cell design is the ratio of electrode length to separator length,  $r$ . Figure 9 plots concentration as a function of time at the center of the electrode for four different values of  $r$ . A large value of  $r$  corresponds to a relatively short separator, which allows Li ions to rapidly diffuse into the electrode. Therefore, this will make the influx of Li ions to be higher when compared to the lower ratio cases. This is the reason why the concentration profile is highest for  $r = 10$  and lowest for  $r = 3$ . It is interesting to note that for small values of  $r$ , the model predicts rapid reduction in concentration with time initially, resulting in a minima, which is followed by a gradual rise in concentration at later times.

## Conclusions

Concentration-dependent pore wall flux assumed in this work may be more appropriate than the standard assumption of constant and uniform pore wall flux over a larger range of parameters for the modeling of solution phase limitation in a Li-ion cell. This work presents a general framework in which to consider concentration-dependent pore wall flux and specifically analyzes the problem where pore wall flux is linearly proportional to the local concentration. This case is shown to result in a non-linear integro-differential equation, for which, an appropriate linearization technique is discussed.

In the present paper, validation of the theoretical model is limited to comparison with numerical simulation results, and comparison with results from past work based on a constant reaction rate assumption. While these are shown to provide reasonable results, in contrast, direct experimental validation of the present work through measurement of concentration field in the electrode stack may be considerably difficult. The theoretical work presented here is to be seen as an intermediate step towards ultimately predicting the charge/discharge characteristics of the cell. It is expected that prediction of charge/discharge characteristics of the cell based on this work may be more easily validated through measurements.

Key limitations of the present model include the assumption of isothermal conditions, which may break down at large discharge rates. Further, diffusion coefficients are assumed to be independent of concentration, and effective diffusivity in the electrode is modeled using assumed values of the Bruggemann coefficient. Finally, constant

current conditions are assumed, whereas, significant variation in current with time may be encountered in realistic scenarios. The time-dependence of current can, in principle, be accounted for through analytical tools such as Green's functions.<sup>16,21</sup>

In addition to expanding the theoretical understanding of species transport in a Li-ion cell under solution phase limitation, the results from this work may also contribute towards optimization of Li-ion cell design for practical applications.

### Acknowledgments

This material is based upon work supported by CAREER Award No. CBET-1554183 from the National Science Foundation.

### ORCID

Ankur Jain  <https://orcid.org/0000-0001-5573-0674>

### References

- B. Scrosati and J. Garche, "Lithium batteries: status, prospects and future." *J. Power Sources*, **195**, 2419 (2010).
- V. Etacheri, R. Marom, R. Elazari, G. Salitra, and D. Aurbach, "Challenges in the development of advanced Li-ion batteries: a review." *Energy Environ. Sci.*, **4**, 3243 (2011).
- T. Kim, W. Song, D. Y. Son, L. K. Ono, and Y. Qi, "Lithium-ion batteries: outlook on present, future, and hybridized technologies." *J. Mater. Chem. A*, **7**, 2942 (2019).
- Y. Xing, E. W. Ma, K. L. Tsui, and M. Pecht, "Battery management systems in electric and hybrid vehicles." *Energies*, **4**, 1840 (2011).
- K. Shah, N. Balsara, S. Banerjee, M. Chintapalli, A. P. Cocco, W. K. S. Chiu, and A. Jain, "State of the art and future research needs for multiscale analysis of Li-ion cells." *J. Electrochem. Energy Conversion & Storage*, **14**, 020801 (2017).
- J. Zhang and J. Lee, "A review on prognostics and health monitoring of Li-ion battery." *J. Power Sources*, **196**, 6007 (2011).
- A. Jokar, B. Rajabloo, M. Désilets, and M. Lacroix, "Review of simplified Pseudo-two-Dimensional models of lithium-ion batteries." *J. Power Sources*, **327**, 44 (2016).
- R. Xiong, J. Cao, Q. Yu, H. He, and F. Sun, "Critical review on the battery state of charge estimation methods for electric vehicles." *IEEE Access*, **6**, 1832 (2018).
- G. G. Botte, V. R. Subramanian, and R. E. White, "Mathematical modeling of secondary lithium batteries." *Electrochim. Acta*, **45**, 2595 (2000).
- J. Newman and K. E. Thomas-Alyea, *Electrochemical Systems*. (Wiley, New York, NY) (2012).
- T. F. Fuller and J. A. Newman, "Concentrated solution theory model of transport in solid-polymer-electrolyte fuel cells." *Electrochem. Soc. Proc*89 (1989).
- V. Ramadesigan, V. Boovaragavan, J. C. Pirkle Jr., and V. R. Subramanian, "Efficient reformulation of solid-phase diffusion in physics-based lithium-ion battery models." *J. Electrochem. Soc.*, **157**, A854 (2010).
- V. R. Subramanian, V. Boovaragavan, V. Ramadesigan, and M. Arabandi, "Mathematical model reformulation for lithium-ion battery simulations: Galvanostatic boundary conditions." *J. Electrochem. Soc.*, **156**, A260 (2009).
- M. Doyle and J. Newman, "Analysis of capacity-rate data for lithium batteries using simplified models of the discharge process." *J. Appl. Electrochem.*, **27**, 846 (1997).
- M. Guo, G. Sikha, and R. E. White, "Single-particle model for a lithium-ion cell: thermal behavior." *J. Electrochem. Soc.*, **158**, A122 (2010).
- M. Parhizi, M. Pathak, and A. Jain, "Analytical model based prediction of state-of-charge (SoC) of a lithium-ion cell under time-varying charge/discharge currents." *J. Electrochem. Soc.*, **167**, 120544 (2020).
- X. Han, M. Ouyang, L. Lu, and J. Li, "Simplification of physics-based electrochemical model for lithium ion battery on electric vehicle. Part I: Diffusion simplification and single particle model." *J. Power Sources*, **278**, 802 (2015).
- V. R. Subramanian and R. E. White, "New separation of variables method for composite electrodes with galvanostatic boundary conditions." *J. Power Sources*, **96**, 385 (2001).
- S. Atlung, K. West, and T. Jacobsen, "Dynamic aspects of solid solution cathodes for electrochemical power sources." *J. Electrochem. Soc.*, **126**, 1311 (1979).
- S. H. Ali, A. Hussin, and A. K. Arof, "Short-and long-time solutions for material balance equation in lithium-ion batteries by Laplace transform." *J. Power Sources*, **112**, 435 (2002).
- M. Parhizi and A. Jain, "Analytical modeling of solid phase diffusion in single-layer and composite electrodes under time-dependent flux boundary condition." *J. Electrochem. Soc.*, **167**, 060528 (2020).
- T. R. Tanim, C. D. Rahn, and C. Y. Wang, "A reduced order electrolyte enhanced single particle lithium ion cell model for hybrid vehicle applications." *American Control Conference (IEEE)* p. 141 (2014).
- W. Luo, C. Lyu, L. Wang, and L. Zhang, "A new extension of physics-based single particle model for higher charge-discharge rates." *J. Power Sources*, **241**, 295 (2013).
- V. R. Subramanian, D. Tapriyal, and R. E. White, "A boundary condition for porous electrodes." *Electrochem. & Solid State Lett.*, **7**, A259 (2004).
- A. Guduru, P. W. Northrop, S. Jain, A. C. Crothers, T. R. Marchant, and V. R. Subramanian, "Analytical solution for electrolyte concentration distribution in lithium-ion batteries." *J. Appl. Electrochem.*, **42**, 189 (2012).
- M. R. Johan and A. K. Arof, "Modeling of electrochemical intercalation of lithium into a LiMn<sub>2</sub>O<sub>4</sub> electrode using green function." *J. Power Sources*, **170**, 490 (2007).
- M. Parhizi and A. Jain, "Analytical modeling of solution-phase diffusion in porous composite electrodes under time-dependent flux boundary conditions using Green's function method." *Ionics*, **27**, 213 (2021).
- T. F. Fuller, M. Doyle, and J. Newman, "Relaxation phenomena in lithium-ion-insertion cells." *J. Electrochem. Soc.*, **141**, 982 (1994).
- R. B. Bird, W. E. Stewart, and E. N. Lightfoot, *Transport Phenomena* (Wiley, New York, NY) 2nd ed. (2006).
- K. J. Hollenbeck, "INVLAP.M: a matlab function for numerical inversion of laplace transforms by the de Hoog algorithm." (1998), <http://isva.dtu.dk/staff/karl/invlap.htm>, accessed 1/1/2012.
- F. R. de Hoog, J. H. Knight, and A. N. Stokes, "An improved method for numerical inversion of laplace transforms. S.I.A.M." *SIAM J. Sci. & Statistical Comput.*, **3**, 357 (1982).